



Temporally-regulated quick activation and inactivation of Ras is important for olfactory behaviour

SUBJECT AREAS:
NEUROIMAGING
BEHAVIOUR
SENSORY SYSTEMS
IMAGING

Takayuki Uozumi^{1*}, Takaaki Hirotsu^{1*}, Kazushi Yoshida², Ryuji Yamada¹, Akiya Suzuki¹, Gun Taniguchi¹, Yuichi Iino² & Takeshi Ishihara¹

¹Department of Biology, Graduate school of Sciences, Kyushu University, Fukuoka 812-8581, Japan, ²Department of Biophysics and Biochemistry, Graduate School of Sciences, The University of Tokyo, Tokyo 113-0032, Japan.

Received
23 January 2012

Accepted
22 June 2012

Published
9 July 2012

Correspondence and requests for materials should be addressed to T.H. (hirotsu.takaaki.056@m.kyushu-u.ac.jp)

* These authors contributed equally to this work.

Responses to environmental stimuli are mediated by the activation and inactivation of various signalling proteins. However, the temporal dynamics of these events in living animals are not well understood. Here we show real-time imaging of the activity of the key regulator of the MAP kinase pathway, Ras, in living *Caenorhabditis elegans* and that Ras is transiently activated within a few seconds in olfactory neurons in response to increase in the concentration of odorants. This fast activation of Ras is dependent on the olfactory signalling pathway and Ras guanyl nucleotide-releasing protein (RasGRP). A negative feedback loop then quickly leads to Ras inactivation despite the continued presence of the odorant. Phenotypes of Ras mutants suggest this rapid activation and inactivation of Ras is important for regulation of interneuron activities and olfactory behaviours. Our results reveal novel kinetics and biological implication of transient activation of Ras in olfactory systems.

Living organisms employ various signal transduction pathways to react and adapt to environmental change. These signalling pathways are activated or inactivated in response to extracellular or intracellular stimuli and trigger cellular reactions including gene expression, cell survival, apoptosis and many biological responses¹. Signalling proteins play major roles in such events and constantly alter their status in response to continuous environmental stimuli. However, temporal dynamics of the signalling proteins in living organisms is largely unknown, even though observation of signalling proteins' activity *in vivo* is essential for understanding functions and regulatory mechanisms of signal transduction pathways.

Ras-MAP kinase pathway is one of the key signal transduction cascades and regulates cell growth, proliferation, differentiation, neuronal plasticity and others²⁻⁴. Ras belongs to the small G-protein family and functions as a molecular switch, assuming either the GDP-bound inactive form or the GTP-bound active form. Mutations of Ras signalling cause many syndromes and diseases, including cancer⁵. In most cases, Ras is activated in the order of minutes by a guanine nucleotide exchange factor (GEF)⁶⁻⁸ and then activates the MAPK pathway to regulate gene expression. The Ras-MAPK pathway is conserved also in *Caenorhabditis elegans*, contributing to vulval induction and the other multiple developmental events⁹. Recently, it has been reported that the Ras-MAPK pathway also plays important roles in the olfactory system of *C. elegans*^{10,11}. The pathway regulates olfactory sensation in olfactory neurons and olfactory plasticity in interneurons^{10,11}. In olfactory neurons of *C. elegans*, odorants are sensed by olfactory receptors and these odorant signals are transmitted by G-protein α , guanylate cyclase and cGMP-gated channels¹²⁻¹⁶. Our previous immunohistochemical study revealed that MAPK is activated downstream of this olfactory signalling pathway within 10 seconds after an odorant stimulus in olfactory neurons¹¹. This result suggests the possibility that Ras is also quickly activated in the order of seconds in olfactory neurons, which is distinct from the previously reported kinetics of the Ras activation by growth factors. However, there are as yet poor understandings about dynamics, regulatory mechanisms and biological implication of the Ras activity in the olfactory system, because the activity of Ras has not yet been observed in living animals.

In this paper, we performed real-time *in vivo* imaging of the activity of Ras protein and showed quick activation of Ras in response to increase in the concentration of odorants in olfactory neurons in *C. elegans*. Our study revealed that a negative feedback mechanism downstream of the MAPK pathway leads to quick inactivation of Ras, even when the odorant stimulation is continued. This activation and inactivation of Ras occurs within a few seconds, which is an unprecedented fast dynamics of Ras activity. Furthermore, measurements of neural activity



by calcium imaging show that Ras signalling in olfactory neurons modulates activity of interneurons which receive synaptic inputs from the olfactory sensory neurons. Finally, behavioural analyses demonstrate that activation and inactivation of Ras is important for klinotaxis, which is one of the tactics of olfactory behaviour. Our results reveal novel kinetics of Ras activity and biological significance of the transient activation of Ras in the olfactory system.

Results

C. elegans senses various odorants and shows attractive or aversive chemotactic behaviour¹⁷. As previously reported¹¹, mutations in genes involved in the Ras–MAPK kinase (MAPK) pathway cause defects in chemotaxis to attractive odorants. For example, mutant animals show decreased chemotaxis to isoamyl alcohol, which is sensed by AWC olfactory neurons^{17,18} (Fig. 1a). MAPK is activated within 10 sec by odorant stimuli in the AWC neurons, and the activity of the Ras–MAPK pathway in AWC is important for behavioural response to the odour¹¹. Constitutive activation of LET-60 Ras in the *let-60(n1046gf)* mutant, which carries the G13E mutation¹⁹, also reduces olfactory responses¹¹ (Fig. 1a). This suggests that both the activation and inactivation of Ras are important for olfaction; however, the relationship between the dynamics of Ras activation/inactivation and olfactory behaviours remains unclear.

To assess the temporal profile of Ras activation, we expressed Raichu-Ras—a Förster resonance energy transfer-based biosensor consisting of yellow fluorescent protein (YFP) and cyan fluorescent protein (CFP)²⁰ (Supplementary Fig. S1)—in AWC neurons using the *odr-1* promoter²¹, which allowed us to perform *in vivo* imaging of Ras activity. Raichu-Ras fluorescence was detected in regions near the plasma membrane of AWC dendrites, axons, and cell bodies (Supplementary Fig. S2a). The transgenic strain did not show any defects in chemotaxis to isoamyl alcohol, suggesting that the AWC olfactory neurons expressing Raichu-Ras functioned normally (Supplementary Fig. S2b). To image Raichu-Ras signals, transgenic animals were glued on agarose pads, placed into a perfusion chamber and covered with buffer. Then diluted isoamyl alcohol was added to the buffer (see Methods). Imaging clearly showed an increase in the YFP/CFP emission ratio near the AWC membranes within a few seconds after addition of isoamyl alcohol (Fig. 1b, e, Supplementary movie S1). After reaching the peak, the ratio decreased to the basal value within 2–3 sec even if the odorant was still present (Fig. 1b, e). These transient changes in the ratio were reproducibly observed with similar kinetics (Fig. 1b, Supplementary Fig. S3). The changes in YFP and CFP fluorescence intensities opposed each other (Fig. 1b), and ratio changes were not observed when mutant types of Raichu-Ras (m001, m102, m103) were used (Fig. 1c, Supplementary Fig. S4a, b, d); m001 lacks Raf RBD; m102 contains Y40C mutation in Ras leading to inhibit the interaction of Ras with Raf; m103 contains S17N mutation reducing the affinity of guanine nucleotides²⁰, which are good indications that the changes in the ratio reflected Ras activity, rather than being an artefact (Fig. 1b). In contrast, no ratio changes were detected following application of only the solvent, ethanol or pyrazine, which is sensed by AWA olfactory neurons (Fig. 1d, Supplementary Fig. S4c, d). Ras activation was repeatedly observed after two or three stimulations with stepwise increases of odorant concentration (Fig. 1f). On the contrary, sham stimuli that did not affect final concentration of the odour failed to activate Ras (Supplementary Fig. S5). These results demonstrate that Ras is transiently activated owing to an increase in the odorant concentration, implying that the Ras activation/inactivation may be temporally regulated.

In the AWC neurons, odorants are thought to be sensed by seven-transmembrane G protein-coupled receptors and lead to either opening or closure of cyclic nucleotide-gated channel via cyclic GMP second messenger². Our previous report suggested that Ras is activated downstream of the olfactory sensory signalling¹¹. To verify

that Ras activation depends on the pathway *in vivo*, we monitored Ras activity using Raichu-Ras in *odr-3(n2150)* and *tax-2(ks10)* mutants. *odr-3* and *tax-2* encode components of olfactory signalling in AWC neurons: a G protein alpha subunit and a cyclic GMP-gated channel beta subunit, respectively^{12,16}. In the *odr-3* and *tax-2* mutants, Ras activation was not detected after application of isoamyl alcohol (Fig. 2a, b, f). These results suggest that Ras is activated by odorant stimuli downstream of the olfactory sensory signalling in the AWC neurons.

It is widely known that activation of Ras is directly mediated by a Ras-guanine nucleotide exchange factor (Ras-GEF), which catalyzes the replacement of Ras-bound GDP by GTP⁶. *C. elegans* has multiple putative Ras-GEF genes. Among them, SOS-1 has been reported to function as a Ras-GEF during vulval induction and other processes⁹ (Supplementary Fig. S6). SOS-1 was required for olfactory plasticity (Supplementary Fig. S7), a process previously reported to be regulated by the Ras–MAPK pathway¹⁰. *sos-1(cs41)* mutants, however, showed normal chemotaxis to isoamyl alcohol (Fig. 1a). Recently, it has been reported that RGEF-1, an ortholog of mammalian RasGRP, is required for MAPK activation in olfactory neurons in response to odorant stimuli²². *rgef-1(ok675)* mutants exhibited significant defects in chemotaxis to isoamyl alcohol (Fig. 1a), and *rgef-1* expression in the AWC neurons rescued the defects (Supplementary Fig. S8), as shown in the previous report²², confirming that RGEF-1 functions in AWC olfactory neurons. In the *rgef-1(ok675)* mutants, Ras activation was not observed in the AWC neurons (Fig. 2c, f), providing direct evidence that RGEF-1 functions as a Ras-GEF during olfactory reception *in vivo*. The *rgef-1* mutants showed normal olfactory plasticity (Supplementary Fig. S7), suggesting that different Ras-GEFs mediate olfactory reception and plasticity in the *C. elegans* olfactory system (Supplementary Fig. S6b).

The previous report suggested that a diacylglycerol (DAG) signal transports RGEF-1 to membrane regions and activates RGEF-1²². EGL-8 (PLC β) and EGL-30 (G α q) are known to be involved in DAG generation and MAPK activation after odour stimuli was significantly reduced in the *egl-8(n488null)* and *egl-30(ad806lf)* mutants²². To investigate whether DAG signals are also important for quick activation of Ras, we monitored Ras activity in the *egl-8(n488)* and *egl-30(ad806)* mutants. In these mutants, Ras activation was greatly reduced, but we noticed that weak but significant activation was reproducibly observed (Fig. 2d–f). These results are qualitatively distinct from that of the *rgef-1* mutants, in which no consistent Ras activation was observed (Fig. 2c, f). Therefore both the DAG signal and another signal downstream of odour reception are important for regulation of quick activation of Ras via RGEF-1.

As mentioned above, *let-60(n1046gf)* mutants showed reduced olfactory behaviour¹¹ (Fig. 1a), indicating that regulation of Ras inactivation is important. Ras activity quickly returned to the basal level within 2–3 sec after the peak Ras activation, even though the calcium level continued to decrease (Fig. 1b, Supplementary Fig. S3, S9). Therefore, such quick inactivation of Ras suggests the presence of negative feedback mechanisms. Our previous study demonstrated that MAPK is activated by isoamyl alcohol stimulus in the AWC neurons downstream of Ras¹¹. Thus, to investigate whether negative feedback mechanisms downstream of Ras modulate Ras inactivation, we analyzed Ras activity in the mutants of *mpk-1*, which encodes MAPK in *C. elegans*²³. In the *mpk-1(ga117null)* mutants, Ras was normally activated within a few seconds after odour stimulation, but activation longer than that of wild-type animals was observed (Fig. 3a). Indeed, the average time to peak Ras activation was similar in *mpk-1* mutants and wild-type animals, whereas the average duration of activation was longer in *mpk-1* mutants (Fig. 3b). These results suggest that quick inactivation of Ras is regulated by a negative feedback loop downstream of MAPK.

Our previous report suggested that MAPK is activated by odour stimuli in AIY interneurons and probably regulates olfactory

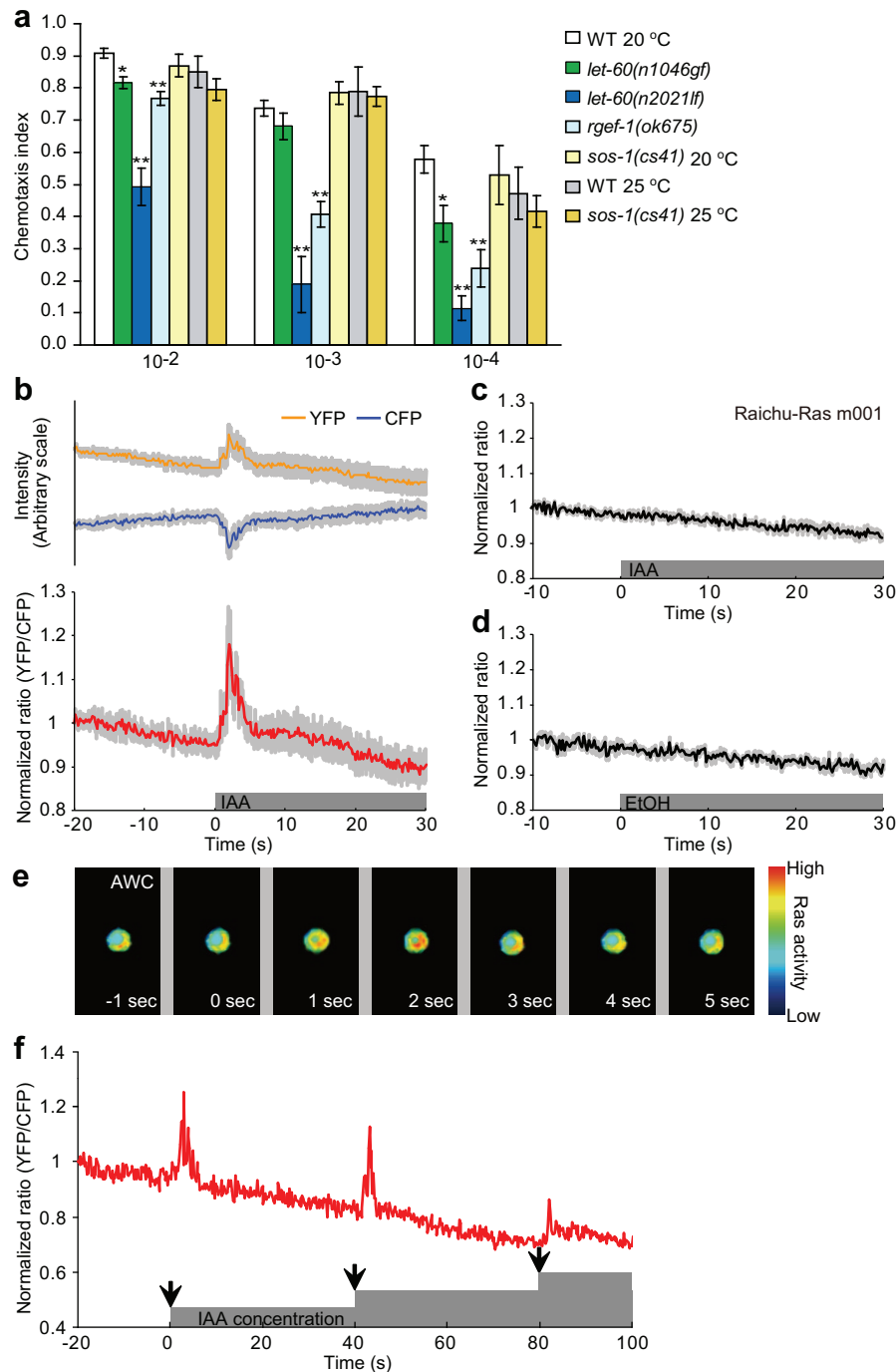


Figure 1 | Ras is transiently activated in olfactory neurons in response to increased odorant concentrations. (a) Chemotaxis to isoamyl alcohol in wild-type (WT) worms, *let-60* mutants, *rgef-1* (Ras-GRP) and *sos-1* (SOS) mutants ($n \geq 6$ assays). All strains were cultured at 20°C except for the temperature sensitive strain *sos-1(cs41)^{ts}* and a wild-type control, which were cultured also at 25°C for 24 hrs before the assays. Isoamyl alcohol dilutions are indicated below the graph. Error bars indicate SEM and asterisks indicate significant differences compared with wild-type animals (* $P < 0.05$, ** $P < 0.01$; Dunnett's test). (b) Temporal profiles of YFP and CFP fluorescence and the mean intensity ratio (YFP/CFP) of Raichu-Ras in AWC neurons after application of isoamyl alcohol (IAA) ($n = 8$). The shaded region around the plotted data represents SEM. (c) Mean intensity ratio of Raichu-Ras m001 (a mutant type of Raichu-Ras) after application of IAA ($n = 8$). (d) Mean intensity ratio of Raichu-Ras after stimulation with ethanol (EtOH) ($n = 5$). (e) Images of an AWC cell body expressing Raichu-Ras. Colours indicate values of the YFP/CFP intensity ratio, with a high ratio (red) corresponding to high Ras activity. (f) Representative Ras activity in AWC after repeated stimulation with IAA. Filled arrows represent an increase in the concentration of IAA. The final dilutions of the odorant are 5×10^{-4} , 1×10^{-3} , and 1.5×10^{-3} after the first, second, and third stimulation, respectively.

plasticity¹⁰, indicating a possibility that functions of MAPK in AIY may affect Ras activity in AWC, because interneuron-mediated feedback regulation of AWC has been reported previously²⁴. To elucidate whether the quick inactivation of Ras in AWC is controlled by functions of MAPK in AWC sensory neurons or those in AIY

interneurons, we analyzed effects of knockdown of *mpk-1* functions in AWC or AIY on the Ras activity in AWC. As a result, knockdown of *mpk-1* functions in AWC of wild type caused significantly longer duration of the Ras activation, whereas AIY-specific knockdown of *mpk-1* functions did not affect the Ras inactivation (Fig. 3b,

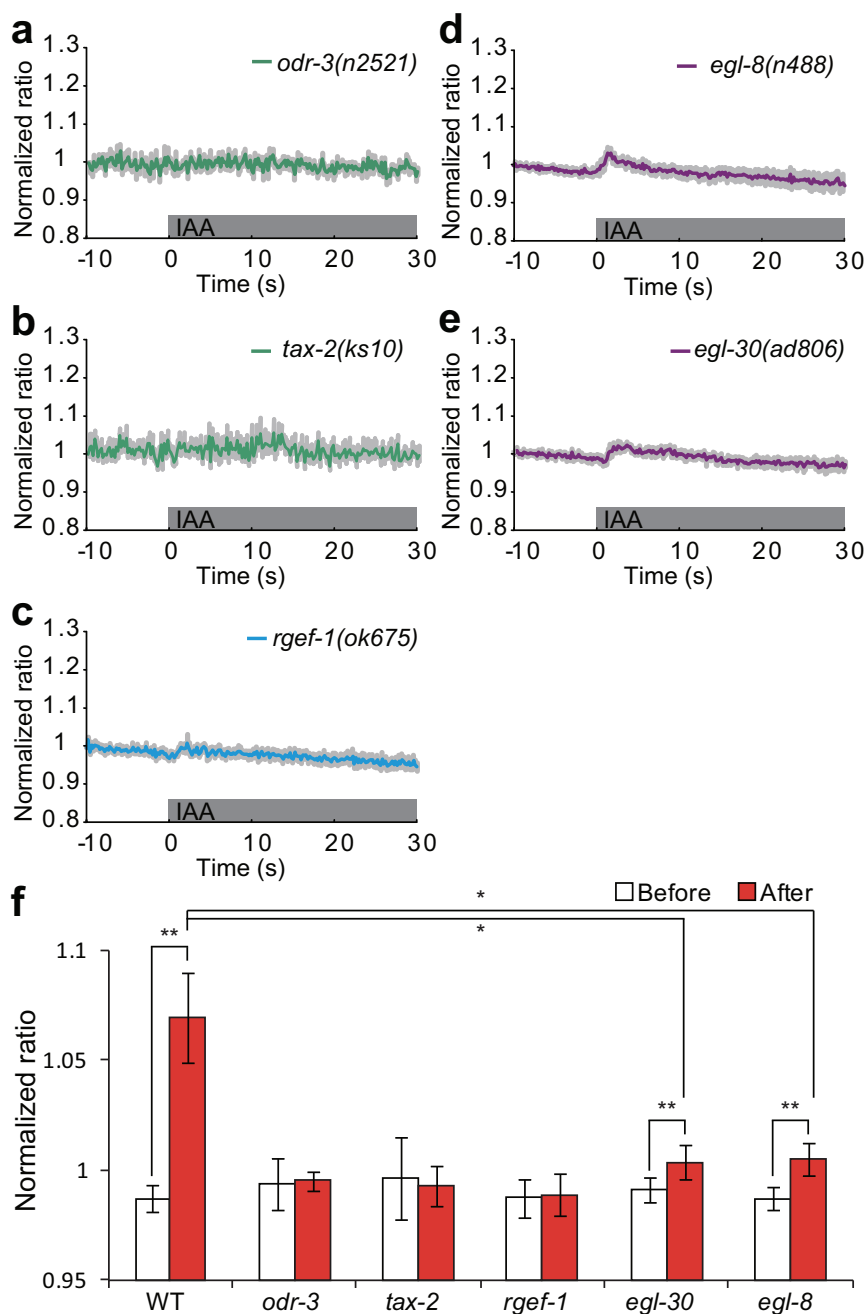


Figure 2 | Regulation of Ras activation in AWC olfactory neurons. (a–e) Isoamyl alcohol-induced Ras activation in the AWC neurons of *odr-3(n2521)* (n = 12) (a), *tax-2(ks10)* (n = 8) (b), *rgef-1(ok675)* (n = 8) (c), *egl-8(n488)* (n = 9) (d), and *egl-30(ad806)* mutants (n = 7) (e). The shaded region around the plotted data represents SEM and each stimulus was applied at 0 sec. (f) Average ratio changes of Raichu-Ras in wild type and several mutants during the 5 sec before and after odour stimulation. Error bars indicate SEM and asterisks indicate significant differences (* $P < 0.05$; Dunnett's test, ** $P < 0.01$; Student's t test).

Supplementary Fig. S10). These results suggest that the inactivation kinetics of Ras is controlled by the MAPK functions in AWC.

To clarify the role of MPK-1, we tested chemotaxis of *mpk-1* mutants. The *mpk-1(ga117null)* mutants showed severe defects in chemotaxis to isoamyl alcohol (Fig. 3c). The defect of the *mpk-1* mutants was severer than that of *let-60(lf)* mutants, probably because *mpk-1(ga117)* is a null mutant. The chemotaxis defect of the *mpk-1* mutants was fully rescued by expression of *mpk-1* in the AWC neurons but not in AIY interneurons (Fig. 3d). Knockdown of *mpk-1* functions in AWC caused a severe chemotaxis defect similar to the *mpk-1* mutants (Fig. 3e). These results suggest that MPK-1 regulates olfactory transduction in the AWC olfactory neurons, possibly by sending olfactory signals to downstream factors and by sending

negative feedback signal to Ras. In conclusion, the Ras activation is regulated by RGEF-1 downstream of the olfactory sensory signalling and the DAG signal, and the quick Ras inactivation is controlled by a negative feedback loop involving MPK-1 in the AWC neurons (Fig. 3f).

To assess behaviours that are regulated by activation and inactivation of Ras, we next monitored chemotaxis behaviours of *let-60* mutants in detail. *C. elegans* swimming toward an attractive odorant is attained of two types of elementary behaviours: klinotaxis and klinokinesis^{25,26} (Supplementary Fig. S11a, b). We quantified klinotaxis and klinokinesis using the weathervane index and pirouette index, respectively (see Methods). In our assay, these behaviours were only observed near the odorant (within 30 mm of the odorant)

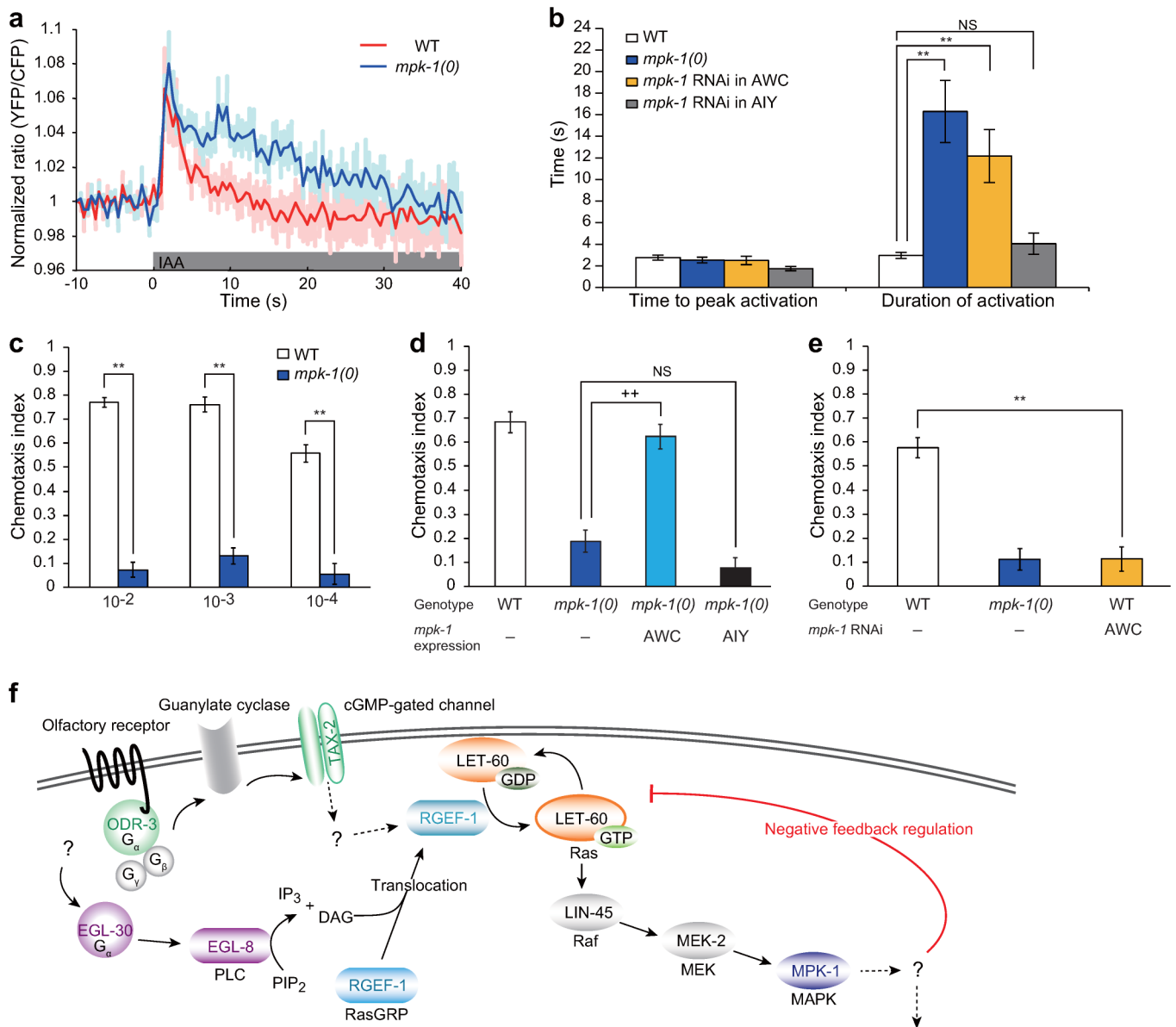


Figure 3 | Negative feedback loop controls quick inactivation of Ras. (a) Ras activity in the AWC neurons in response to 5×10^{-4} dilution of IAA in wild type (WT) ($n = 10$) and *mpk-1(gal17null)* mutants ($n = 9$). The shaded region around the plotted data represents SEM. (b) Average time to peak of Ras activation and average duration of Ras activation in wild type ($n = 10$), the *mpk-1* mutants ($n = 9$) and wild type with knockdown of *mpk-1* functions in AWC ($n = 9$) or AIY ($n = 10$). The period between stimulation and peak Ras activation was defined as the ‘time to peak activation’ whereas the period between the peak and a return to the basal ratio value (mean ratio during 10 sec preceding the first application of IAA) was defined as the ‘duration of activation’. Error bars indicate SEM and the asterisks indicate significant differences compared with wild-type samples (** $P < 0.01$; Dunnett’s test). (c) Chemotaxis to isoamyl alcohol (IAA) in wild type and *mpk-1(gal17)* mutants ($n \geq 6$ assays). IAA dilutions are indicated below the graph. (d) Chemotaxis to 10^{-3} dilution of IAA of the *mpk-1* mutants expressing *mpk-1* cDNA in AWC sensory neurons by the *odr-1* promoter or AIY interneurons by the AIY-specific *ttx-3* promoter ($n \geq 4$ assays). (e) Chemotaxis to 10^{-4} dilution of IAA of wild type with knockdown of *mpk-1* functions in AWC ($n \geq 5$ assays). Error bars indicate SEM and significant differences are indicated by ** ($P < 0.01$; Student’s t test) and ++ ($P < 0.01$; Dunnett’s test). NS; not significant ($P > 0.05$). (f) A model of the regulation of the Ras activity in the AWC sensory neurons. Previous reports revealed that EGL-8 (PLC β) generates diacylglycerol (DAG) and the DAG signal transports RGEF-1 (RasGRP) to membrane regions. Quick activation of Ras via RGEF-1 is mediated by the signal from olfactory sensory signaling and the DAG signal. After activation, Ras is quickly inactivated by negative feedback mechanisms downstream of MPK-1 (MAPK).

(Fig. 4a, b). As for klinotaxis, both *let-60(n1046gf)* and *let-60(n2021lf)* mutants showed severe defects (Fig. 4a), indicating that proper regulation of Ras activity is essential for regulation of this behavioural mechanism. The *mpk-1(gal17null)* mutants also exhibited obvious defects in klinotaxis behaviour (Supplementary Fig. S12). On the other hand, klinokinesis was partially impaired in the *let-60(gf)* and *let-60(lf)* mutants (Fig. 4b). Of note, these defects may reflect, at least in part, an abnormal basal pirouette frequency under odour-free

conditions (Fig. 4c). Therefore, though Ras signalling may also be involved in klinokinesis, these observations indicate that Ras activity clearly regulates klinotaxis behaviour, in which Ras activation in response to increased odour concentrations upon head swing may contribute to the curving behaviour toward the odourant.

Our results revealed that impaired Ras activation and inactivation cause abnormal behavioural phenotypes. Next, we sought to determine how Ras signalling affects the activity of the neural circuit that

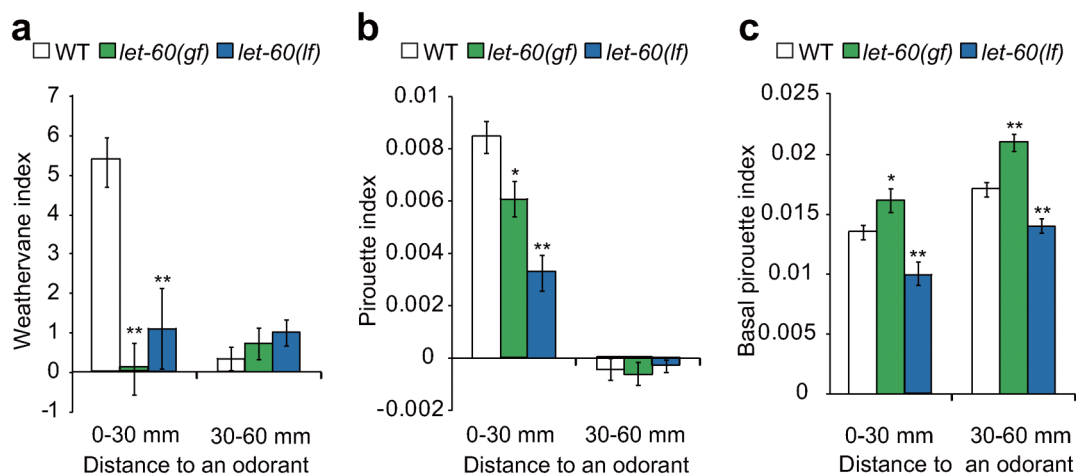


Figure 4 | Ras signalling regulates klinotaxis behaviour. Klinotaxis (a), klinokinesis (b), and the basal pirouette index (c) in wild-type (WT), *let-60(n1046gf)*, and *let-60(n2021lf)* animals during chemotaxis to isoamyl alcohol at a dilution of 10^{-4} . $n = 12$ for WT, 11 for *let-60(gf)*, and 10 for *let-60(lf)*. Error bars represent SEM. Significant differences compared with wild-type animals are indicated (* $P < 0.05$, ** $P < 0.01$; Dunnett's test).

regulates olfactory behaviours. We used calcium imaging to monitor the activities of AIB interneurons, which receive synaptic inputs from AWC neurons and regulate olfactory behaviours^{18,25}. In AIB neurons, Ca^{2+} concentrations decreased in response to odour stimuli (Fig. 5a, g, k), as previously reported¹⁸. In the *let-60(gf)* mutants, the AIB response was not observed (Fig. 5b, k), revealing that constitutive Ras activation disturbed the responses of downstream interneurons. On the other hand, in the *let-60(lf)* mutants, unstable calcium concentrations were observed in AIB neurons in the presence of odour stimuli (Fig. 5c, h). To quantitatively analyze the oscillatory activity of AIB interneurons in the *let-60(lf)* mutants, we used a Fourier transform which is well suited for revealing oscillatory responses. Spectral analysis showed significant increase in the band power in a low-frequency domain (0.03–1.0 Hz) in the *let-60(lf)* mutants compared to wild-type animals (Fig. 5l, Supplementary Fig. S13a, b). These results suggest that Ras signalling may suppress oscillatory AIB activity. In the *let-60* mutants, responses of AWC neurons to odour stimuli measured by calcium imaging were identical to those of wild type, suggesting that Ras signalling is not involved in regulating depolarization of the AWC olfactory neurons themselves (Supplementary Fig. S14).

To investigate where Ras signalling acts to regulate AIB responses, we performed cell-specific rescue experiments. Expression of wild-type *let-60* gene in AWC sensory neurons significantly rescued the oscillatory AIB activity of the *let-60(lf)* mutants (Fig. 5d, i, l). On the other hand, AIB-specific expression of *let-60* did not (Fig. 5e, j, l). Furthermore, overexpression of *let-60* in AWC prevented the responses of AIB, in a manner similar to the *let-60(gf)* mutants (Fig. 5f, k). These results demonstrate that Ras signalling in the AWC sensory neurons affects the responses of downstream interneurons, which likely leads to abnormal olfactory behaviours.

It was previously reported that the transmembrane guanylyl cyclase GCY-28 and axonal diacylglycerol (DAG) signalling through the protein kinase C (PKC-1) regulate synaptic outputs of the AWC sensory neurons and the activity of AIB interneurons²⁷. In *gcy-28* mutants, a calcium decrease in AIB after addition of butanone was not observed. Therefore, there is a possibility that both Ras signalling and GCY-28/PKC-1 signalling function in the same pathway to regulate the output of AWC and the AIB activity. The putative null mutants of *gcy-28*, *gcy-28(tm2411)*, showed severer defects than the *let-60(n1046gf)* and *let-60(n2021lf)* mutants in chemotaxis to isoamyl alcohol (Fig. 6a). *gcy-28(tm2411)*; *let-60(n1046gf)* and *gcy-28(tm2411)*; *let-60(n2021lf)* double mutants exhibited decreased chemotaxis as much as *gcy-28(tm2411)* single mutants (Fig. 6a). Thus,

GCY-28 may act downstream of Ras signalling. It was previously reported that PKC-1 regulates synaptic transmission and neuropeptide release^{28,29} and that PKC-1 acts downstream of or in parallel to GCY-28 to regulate AWC functions, since constitutive active form of PKC-1 rescued the chemotaxis defects of *gcy-28* mutants²⁷. We observed that expression of *pkc-1(gf)* in AWC also significantly rescued the defects of *let-60* mutants in chemotaxis to isoamyl alcohol (Fig. 6b, c). These results suggest that PKC-1 acts downstream of or in parallel to Ras signalling to regulate output of AWC.

Discussion

In this study, we performed live imaging of the activity of the major signalling protein, Ras, in living animals. Raichu-Ras was previously characterized in cultured cell lines and activation of Ras was observed 15–30 min after stimulation with epidermal growth factors²⁰. Also in a single dendritic spine, Ca^{2+} -dependent Ras activation was observed at the order of minutes, using Fras-F, another FRET-based indicator of Ras activation³⁰. Therefore, our results reveal, for the first time, fast kinetics of activation and inactivation of Ras at the order of seconds.

In contrast to the activation of MAPK within 10 seconds of odour stimuli in AWC neurons¹¹, MAPK is activated 5 min after odour stimuli in interneurons critical for olfactory plasticity¹⁰, and SOS-1 is involved in the plasticity. Our results show that different Ras-GEFs are used for olfactory reception or olfactory plasticity in the olfactory system in *C. elegans*, suggesting that different types of Ras-GEF may be used depending on the time scale of Ras activation. A similar phenomenon is observed in T lymphocytes, where SOS and RasGRP function in parallel in the different time scales^{6,7}.

In response to increase in odour concentrations, Ras is quickly activated and immediately inactivated. For klinotaxis, worms may have to sense changes in the odour concentration during each head swing^{25,31}, during forward locomotion, each head swing occurs over the course of a few seconds, which is consistent with the timescale of transient Ras activation. Thus, the dynamics of Ras activation may help to tune the animal's quick response to changes in odour concentrations during klinotaxis. In *let-60(lf)* mutants, oscillatory neural activity was observed in AIB. Oscillation of Ca^{2+} concentrations was previously observed in the AWC neurons of neuropeptide-deficient mutants²⁴. Therefore, Ras signalling may regulate neuropeptide release to suppress oscillation of AIB neural activity and regulate olfactory behaviours. It was previously reported that PKC-1 regulates neuropeptide release²⁹ and our results suggest that GCY-28 and probably PKC-1 functions downstream of Ras signalling. These

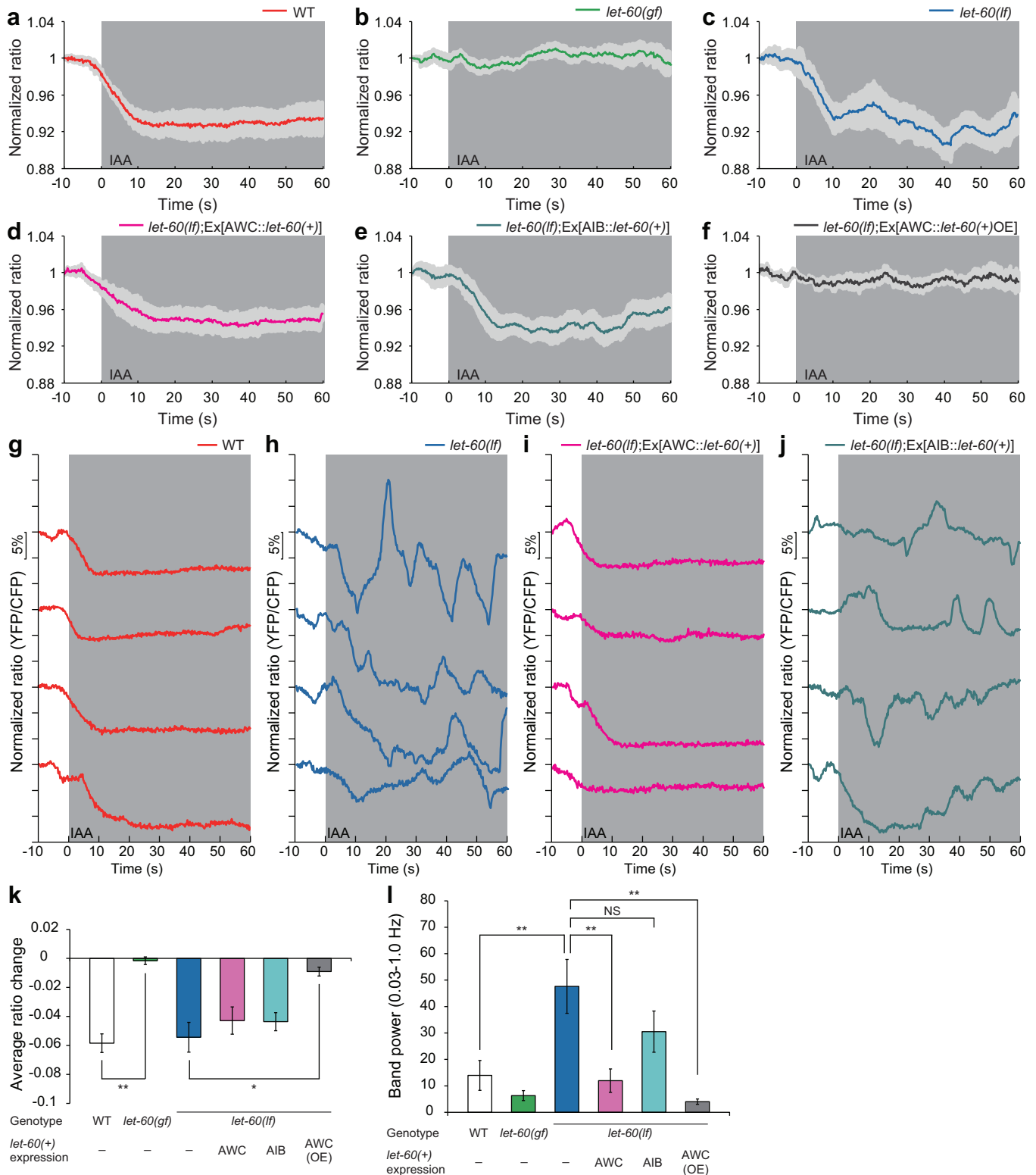


Figure 5 | Ras signalling in AWC olfactory neurons controls the activity of AIB interneurons. (a–c) Mean intensity ratio (YFP/CFP) of YC3.60 in AIB interneurons of wild type ($n = 9$) (a), *let-60(n1046gf)* mutants ($n = 11$) (b), and *let-60(n2021lf)* mutants ($n = 12$) (c) exposed to isoamyl alcohol (IAA) at a dilution of 10^{-4} . (d–f) Mean intensity ratio of YC3.60 in AIB of *let-60(lf)* mutants with expression of *let-60* cDNA in AWC by the *odr-1* promoter ($n = 9$) (d), in AIB by the *npr-9* promoter ($n = 13$) (e), and overexpression of *let-60* in AWC ($n = 7$) (f) after addition of 10^{-4} dilution of IAA. IAA was added at 0 sec and the grey shading indicates the presence of IAA. The coloured shaded regions around the plotted data represent SEM. (g–j) Representative AIB calcium responses in individual wild-type animals (g), *let-60(lf)* mutants (h) and *let-60(lf)* mutants with expression of *let-60* in AWC (i) or AIB (j) after application of IAA at 10^{-4} . (k) Average ratio changes of AIB calcium responses during the 10 sec before and after odour stimulation in wild type, *let-60(gf)* mutants, *let-60(lf)* mutants and *let-60(lf)* mutants with expression of *let-60* in AWC, in AIB, and overexpression of *let-60* in AWC. Average ratio change was calculated as (average normalized ratio value during 30 sec after odour stimulation) – (average normalized ratio value during 10 sec before odour stimulation). Error bars indicate SEM and asterisks indicate significant differences ($*P < 0.05$, $**P < 0.01$; Dunnett’s test). (l) Fourier power analysis of wild type, *let-60(gf)* mutants, *let-60(lf)* mutants and *let-60(lf)* mutants with expression of *let-60* in AWC, in AIB, and overexpression of *let-60* in AWC. The average power of the band (0.03 – 1.0 Hz) across calcium traces in AIB interneurons is shown. Error bars indicate SEM and asterisks indicates significant differences ($**P < 0.01$; Dunnett’s test). NS; not significant.

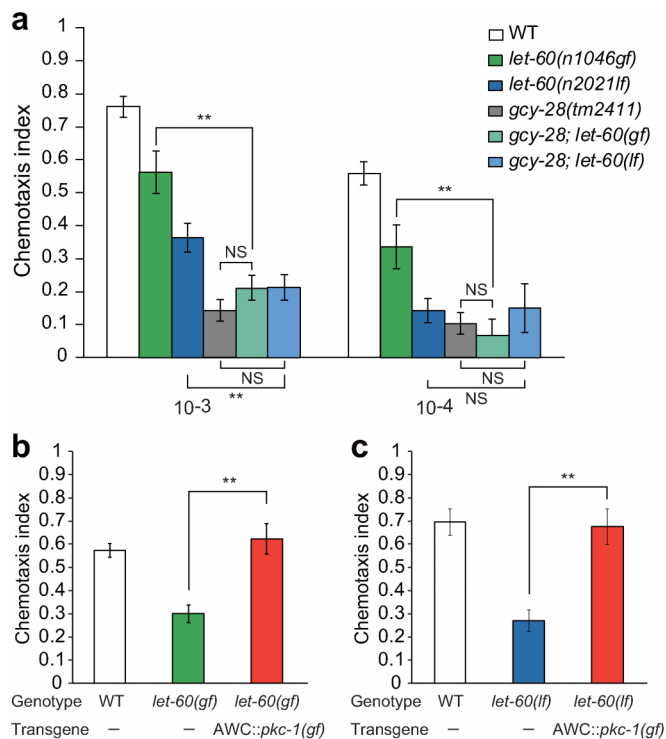


Figure 6 | GCY-28/PKC-1 signalling and Ras signalling function in the same pathway in AWC. (a) Chemotaxis to isoamyl alcohol (IAA) in wild type, *let-60(n1046gf)*, *let-60(n2021lf)*, *gcy-28(tm2411)*, *gcy-28(tm2411); let-60(n1046gf)* and *gcy-28(tm2411); let-60(n2021lf)* mutants ($n \geq 6$ assays). IAA dilutions are indicated below the graph. Error bars indicate SEM and asterisks indicate significant differences (** $P < 0.01$; Student's *t* test with Bonferroni correction). NS; not significant ($P > 0.05$). (b, c) Effect of expression of *pkc-1(gf)* in AWC neurons by the *odr-1* promoter on chemotaxis to IAA of the *let-60(gf)* (b) and *let-60(lf)* mutants (c). IAA dilutions are 10^{-4} (b) and 10^{-3} (c). $n \geq 6$ assays. Error bars indicate SEM and asterisks indicate significant differences (** $P < 0.01$; Student's *t* test).

results may support our idea that Ras signalling controls neuropeptide release of the AWC neurons.

Our imaging analyses reveal that even if odour stimuli were still present, Ras is quickly inactivated within a few second. On the other hand, the activity of MAPK may persist for longer time, because MAPK activation was observed after continuous odour stimulation for 3 min²². Such distinct kinetics between Ras and MAPK suggest the possibility that quick inactivation of Ras may be also required for regulation of different signal cascades from the MAPK pathway to control olfactory behaviours.

Calcium imaging has been widely used in *C. elegans* to examine neural activity in response to various stimuli³². The activities of specific proteins, however, have not yet been observed in living animals of *C. elegans*. Our results provide a foundation for future probes and detection systems that will allow monitoring of the activities of many proteins and their associated temporal regulation in *C. elegans* and other organisms.

Methods

Strains. *C. elegans* were cultured and maintained at 20°C under standard conditions³³, except for the temperature sensitive strain *sos-1(cs41)*, which was cultured at 25°C. The NA22 *E. coli* strain was used as a food source. Wild-type animals were Bristol strain N2. Other strains used in this study included *tax-2(ks10) I*, *egl-30(ad806) I*, *gcy-28(tm2411) I*, *mpk-1(ga117) III*, *let-60(n1046gf) IV*, *let-60(n2021lf) IV*, *sos-1(cs41) V*, *rgef-1(ok675) V*, *odr-3(n2150) V*, and *egl-8(n488) V*.

Plasmid construction and germ-line transformation. Raichu-Ras cDNA (kind gift from M. Matsuda) was inserted downstream of the *odr-1* promoter²¹. Mutant types of Raichu-Ras (m001, m102 and m103) were digested from pRaichu001, pRaichu102

and pRaichu103, respectively and inserted downstream of the *odr-1* promoter²¹. Sequence encoding yellow cameleon (YC) 3.60²² was connected to the *odr-1* or *odr-2* promoter^{21,34}. *rgef-1* cDNA was amplified by *C. elegans* cDNA library. *rgef-1*, *let-60*, *mpk-1* and *pkc-1(gf)* cDNA were inserted downstream of the *odr-1* promoter, *npr-9* promoter or the AIY-specific *ttx-3* promoter for the expression in AWC, AIB or AIY, respectively^{21,35,36}. Germ-line transformations were performed using standard methods³⁷. *lin-44p::GFP* and *myo-3p::GFP* were used as transformation markers. In Fig. 5, *odr-1p::let-60* was injected to the *let-60(lf)* mutants at a concentration of 10 ng/μl for the rescue experiment and 50 ng/μl for the overexpression experiment.

Cell-specific knockdown of *mpk-1* functions. The construction of transgenes to knock down the functions of *mpk-1* gene in a specific neuron was performed as previously reported³⁸. The targeted region of *mpk-1* (1.4-kb genomic sequences) was amplified with two primers Tf = 5'-gttaactcagggtgagga-3' and Tr = 5'-caggattctgcctccatta-3'. *odr-1* and AIY-specific *ttx-3* promoters were used to express the targeted gene in AWC and AIY neurons, respectively.

Ras imaging and analysis. We used Raichu-Ras as probes. Animals that expressed Raichu-Ras in AWC neurons were glued on 4% agarose pads and covered with physiologic buffer solution (80 mM NaCl, 5 mM KCl, 20 mM D-glucose, 10 mM HEPES, 5 mM MgCl₂, and 1 mM CaCl₂ at pH 7.2). Because signals from Raichu-Ras were weak, we did not use a microfluidic device for the analysis owing to the associated noise with this system^{18,39}; animals are able to move in the microfluidic device, which prevented identification of positive signals. Therefore, the measurement of Ras activities after an odour removal was technically difficult. Isoamyl alcohol, which is sensed by AWC neurons, was diluted in ethanol and added to the buffer as the odour stimulus. We confirmed that AWC olfactory neurons responded to the odorant by monitoring Ca²⁺ concentrations under the same conditions used for Ras imaging (Supplementary Fig. S15). The final dilutions of the odorant were 5×10^{-4} , 1×10^{-3} , and 1.5×10^{-3} after the first, second, and third stimulation, respectively. Room temperature was set at 20–23°C. Fluorescent images of Raichu-Ras were obtained using a Zeiss Axioplan 2 microscope equipped with 40× objective lens and ORCA-D2 digital camera (Hamamatsu). Images were collected at an exposure of 200 msec. For long-term analyses of Raichu-Ras fluorescence (Fig. 3a, b, Supplementary Fig. S10), we used a 3CCD digital camera (C7780; Hamamatsu) and all images were collected at an exposure of 500 msec. Similar results were obtained with these two systems (Supplementary Fig. S3). Time stacks of AWC cell bodies were captured and analyzed for the emission ratio of YFP fluorescence to CFP fluorescence using Aqua Cosmos software (ver. 2.6, Hamamatsu). To distinguish weak signals representing Ras activity from noise, we excluded crosstalk between the YFP and CFP emission spectra using a linear unmixing method (Multiband Imaging Software, Hamamatsu). The normalized ratio was calculated as the change in the YFP/CFP ratio relative to the ratio value obtained 10 sec or 20 sec before the odour was applied.

Calcium imaging and statistics. To monitor the responses of AWC and AIB neurons, we generated YC3.60-expressing lines using the *odr-1* and *odr-2* promoters^{21,22,34}, respectively. Calcium imaging of AWC and AIB neurons were performed using a microfluidic device, as described previously^{18,39}, except for Supplementary Fig. S15 in which imaging was performed as described for Ras imaging. For experiments using a microfluidic device, we immobilized each animal by trapping it in a microchannel, such that the nose of the animal was exposed to a flowing stream containing isoamyl alcohol (10^{-4} dilution) or odour-free solution, except for Supplementary Fig. S9 where 10^{-5} and 10^{-7} dilutions of isoamyl alcohol were used. Optical equipment and conditions were similar to the other imaging experiments.

Chemotaxis and olfactory plasticity assays. Chemotaxis assays were performed at 23°C as described previously¹⁷. Isoamyl alcohol was used as an attractive odorant at dilutions of 10^{-3} , 10^{-3} , and 10^{-4} . Olfactory plasticity assays were performed at 23°C as previously described¹⁰. When benzaldehyde was used for assays, the concentration was 10^{-4} for the initial exposure before the experiment and 10^{-2} for odorants spotted on plates. The temperature sensitive strain *sos-1(cs41)*³⁵ and wild-type control animals were cultured at 20°C or 25°C for 24 hrs before the assays, and behavioural assays were performed at 23°C (Fig. 1a, Supplementary Fig. S7). *sos-1(cs41)*³⁵ appeared nearly wild type at 20°C, but had strong larval lethal and vulvaless phenotypes at 25°C⁴⁰. The chemotaxis index was calculated as previously described^{10,17}.

Multiworm tracking system. We used a camera (Lw575M-IO; ARGO Corporation) and LED illumination (HPR-150SW; CCS) equipped with a digital power source (PD2-3024; CCS). Images of 40–100 animals were captured from each assay plate. The interval between image captures was 500 msec, and the recording time was 1 hour. Saved images were analyzed using custom software—based on Lucam Capture software (ARGO Corporation)—that located the centroid of the animals. The design of the plate shown in Supplementary Fig. S11e was used without spotted sodium azide.

Analysis of tracking data. Tracking data was analyzed essentially as described previously²⁵. In a previous report²⁵, data from immotile animals were discarded, whereas tracks shorter than 1 mm were removed from the tracking data in this study. A sharp turn was defined as $> 100^\circ$ change in the direction of locomotion, and consecutive sharp turns separated by less than 3.18 sec were defined as a pirouette. Based on these criteria, locomotion was separated into pirouettes and other tracks



(referred to as runs). Pirouettes were used to quantify klinokinesis, and runs were used to quantify klinotaxis. The direction to the odorant source relative to direction of locomotion and the curving rate were determined as shown in Supplementary Fig. S11c, d. All angles were defined as positive for clockwise rotation.

We calculated the pirouette index, basal pirouette frequency, and weathervane index as previously described²⁵ with some modifications. During klinotaxis, worms respond to a chemical gradient perpendicular to the direction of locomotion²⁵. On the other hand, during klinokinesis, worms respond to a chemical gradient tangential to the direction of locomotion²⁶. Therefore, the sine of bearing (θ) and cosine of bearing were used to quantify klinotaxis and klinokinesis, respectively. In analyses of klinotaxis, the relationship between the sine θ and average curving rate was calculated (Supplementary Fig. S11c). All data points from the tracking data were classified into 10 groups according to the sine θ . The weathervane index was defined as the slope of the regression line, and the average weathervane index for each assay was used for further analyses. In analyses of klinokinesis, the relationship between the cosine θ and the probability of a pirouette was calculated (Supplementary Fig. S11d). All data points from the tracking data were classified into 10 groups according to the cosine θ , and the probability of pirouette initiation was plotted for the midpoint cosine θ in each group. The pirouette index was defined as the negative slope of the regression line. The y intercept of this line is a measure of the basal pirouette frequency, because the direction of locomotion is perpendicular to the odour gradient when cosine θ is 0. The average pirouette index and basal pirouette frequency in each assay are presented.

Fourier analysis. The normalized ratio was calculated as the change in the YFP/CFP ratio relative to the ratio value obtained 10 sec before the odour was applied. Data in the time domain (the normalized ratio trace $y(t)$) were transformed into the frequency domain ($Y(f)$) using a formula;

$$Y(f_k) = \sum_{j=0}^{N-1} e(t_j) e^{-\frac{2\pi i k j}{N}}$$

where $k = 0 \dots N = 256$.

To estimate the total power contributed by oscillatory components in a band bounded by two frequencies f_{\min} and f_{\max} (0.03–1.0, 1.0–3.0, 3.0–5.0 Hz), we calculated integral of energy spectral density as

$$\text{Band power} = \sum_{f_{\min} \leq f_k \leq f_{\max}} |Y(f_k)|^2$$

- Williams, R. J. Signalling: basics and evolution. *Acta Biochim Pol* **51**, 281–298 (2004).
- Mitin, N., Rossmann, K. L. & Der, C. J. Signaling interplay in Ras superfamily function. *Curr Biol* **15**, R563–R574 (2005).
- Karnoub, A. E. & Weinberg, R. A. Ras oncogenes: split personalities. *Nat Rev Mol Cell Biol* **9**, 517–531 (2008).
- Ye, X. & Carew, T. J. Small G protein signaling in neuronal plasticity and memory formation: the specific role of ras family proteins. *Neuron* **68**, 340–361 (2010).
- Malumbres, M. & Barbacid, M. RAS oncogenes: the first 30 years. *Nat Rev Cancer* **3**, 459–465 (2003).
- Buday, L. & Downward, J. Many faces of Ras activation. *Biochim Biophys Acta* **1786**, 178–187 (2008).
- Das, J. *et al.* Digital signaling and hysteresis characterize ras activation in lymphoid cells. *Cell* **136**, 337–351 (2009).
- Omerovic, J., Laude, A. J. & Prior, I. A. Ras proteins: paradigms for compartmentalised and isoform-specific signalling. *Cell Mol Life Sci* **64**, 2575–2589 (2007).
- Sundaram, M. V. RTK/Ras/MAPK signaling. *WormBook*. 2006 Feb **11**, 1–19 (2006).
- Hirotsu, T. & Iino, Y. Neural circuit-dependent odor adaptation in *C. elegans* is regulated by the Ras-MAPK pathway. *Genes Cells* **10**, 517–530 (2005).
- Hirotsu, T., Saeki, S., Yamamoto, M. & Iino, Y. The Ras-MAPK pathway is important for olfaction in *Caenorhabditis elegans*. *Nature* **404**, 289–293 (2000).
- Roayaie, K., Crump, J. G., Sagasti, A. & Bargmann, C. I. The G alpha protein ODR-3 mediates olfactory and nociceptive function and controls cilium morphogenesis in *C. elegans* olfactory neurons. *Neuron* **20**, 55–67 (1998).
- Birnby, D. A. *et al.* A transmembrane guanylyl cyclase (DAF-11) and Hsp90 (DAF-21) regulate a common set of chemosensory behaviors in *Caenorhabditis elegans*. *Genetics* **155**, 85–104 (2000).
- L'Etoile, N. D. & Bargmann, C. I. Olfaction and odor discrimination are mediated by the *C. elegans* guanylyl cyclase ODR-1. *Neuron* **25**, 575–586 (2000).
- Komatsu, H., Mori, I., Rhee, J. S., Akaike, N. & Ohshima, Y. Mutations in a cyclic nucleotide-gated channel lead to abnormal thermosensation and chemosensation in *C. elegans*. *Neuron* **17**, 707–718 (1996).
- Coburn, C. M. & Bargmann, C. I. A putative cyclic nucleotide-gated channel is required for sensory development and function in *C. elegans*. *Neuron* **17**, 695–706 (1996).
- Bargmann, C. I., Hartwig, E. & Horvitz, H. R. Odorant-selective genes and neurons mediate olfaction in *C. elegans*. *Cell* **74**, 515–527 (1993).
- Chalasan, S. H. *et al.* Dissecting a circuit for olfactory behaviour in *Caenorhabditis elegans*. *Nature* **450**, 63–70 (2007).
- Beitel, G. J., Clark, S. G. & Horvitz, H. R. *Caenorhabditis elegans* ras gene *let-60* acts as a switch in the pathway of vulval induction. *Nature* **348**, 503–509 (1990).
- Mochizuki, N. *et al.* Spatio-temporal images of growth-factor-induced activation of Ras and Rap1. *Nature* **411**, 1065–1068 (2001).
- Yu, S., Avery, L., Baude, E. & Garbers, D. L. Guanylyl cyclase expression in specific sensory neurons: a new family of chemosensory receptors. *Proc Natl Acad Sci U S A* **94**, 3384–3387 (1997).
- Chen, L., Fu, Y., Ren, M., Xiao, B. & Rubin, C. S. A RasGRP, *C. elegans* RGEF-1b, couples external stimuli to behavior by activating LET-60 (Ras) in sensory neurons. *Neuron* **70**, 51–65 (2011).
- Lackner, M. R., Kornfeld, K., Miller, L. M., Horvitz, H. R. & Kim, S. K. A MAP kinase homolog, *mpk-1*, is involved in ras-mediated induction of vulval cell fates in *Caenorhabditis elegans*. *Genes Dev* **8**, 160–173 (1994).
- Chalasan, S. H. *et al.* Neuropeptide feedback modifies odor-evoked dynamics in *Caenorhabditis elegans* olfactory neurons. *Nat Neurosci* **13**, 615–621 (2010).
- Iino, Y. & Yoshida, K. Parallel use of two behavioral mechanisms for chemotaxis in *Caenorhabditis elegans*. *J Neurosci* **29**, 5370–5380 (2009).
- Pierce-Shimomura, J. T., Morse, T. M. & Lockery, S. R. The fundamental role of pirouettes in *Caenorhabditis elegans* chemotaxis. *J Neurosci* **19**, 9557–9569 (1999).
- Tsunozaki, M., Chalasan, S. H. & Bargmann, C. I. A behavioral switch: cGMP and PKC signaling in olfactory neurons reverses odor preference in *C. elegans*. *Neuron* **59**, 959–971 (2008).
- Sieburth, D. *et al.* Systematic analysis of genes required for synapse structure and function. *Nature* **436**, 510–517 (2005).
- Sieburth, D., Madison, J. M. & Kaplan, J. M. PKC-1 regulates secretion of neuropeptides. *Nat Neurosci* **10**, 49–57 (2007).
- Harvey, C. D., Yasuda, R., Zhong, H. & Svoboda, K. The spread of Ras activity triggered by activation of a single dendritic spine. *Science* **321**, 136–140 (2008).
- Izquierdo, E. J. & Lockery, S. R. Evolution and analysis of minimal neural circuits for klinotaxis in *Caenorhabditis elegans*. *J Neurosci* **30**, 12908–12917 (2010).
- Dittman, J. Worm watching: imaging nervous system structure and function in *Caenorhabditis elegans*. *Adv Genet.* **65**, 39–78 (2009).
- Brenner, S. The genetics of *Caenorhabditis elegans*. *Genetics* **77**, 71–94 (1974).
- Chou, J. H., Bargmann, C. I. & Sengupta, P. The *Caenorhabditis elegans* odr-2 gene encodes a novel Ly-6-related protein required for olfaction. *Genetics* **157**, 211–224 (2001).
- Bendena, W. G. *et al.* A *Caenorhabditis elegans* allatostatin/galanin-like receptor NPR-9 inhibits local search behavior in response to feeding cues. *Proc Natl Acad Sci U S A* **105**, 1339–1342 (2008).
- Wenick, A. S. & Hobert, O. Genomic cis-regulatory architecture and trans-acting regulators of a single interneuron-specific gene battery in *C. elegans*. *Dev Cell* **6**, 757–770 (2004).
- Mello, C. C., Kramer, J. M., Stinchcomb, D. & Ambros, V. Efficient gene transfer in *C. elegans*: extrachromosomal maintenance and integration of transforming sequences. *EMBO J* **10**, 3959–3970 (1991).
- Esposito, G., Di Schiavi, E., Bergamasco, C. & Bazzicalupo, P. Efficient and cell specific knock-down of gene function in targeted *C. elegans* neurons. *Gene* **395**, 170–176 (2007).
- Chronis, N., Zimmer, M. & Bargmann, C. I. Microfluidics for in vivo imaging of neuronal and behavioral activity in *Caenorhabditis elegans*. *Nat Methods* **4**, 727–731 (2007).
- Rocheleau, C. E. *et al.* A *lin-45* raf enhancer screen identifies *eor-1*, *eor-2* and unusual alleles of Ras pathway genes in *Caenorhabditis elegans*. *Genetics* **161**, 121–131 (2002).

Acknowledgements

We thank the *Caenorhabditis* Genetic Center (CGC) for the strains, M. Matsuda for series of Raichu-Ras probes, A. Miyawaki and T. Nagai for YC3.60, H. Ohno for *mpk-1* cDNA, C. Bargmann for *pkc-1(gf)* cDNA, T. Teramoto for imaging constructs and strains, R. Iritani for the Fourier analysis, H. Tachida for useful advice, and members of our laboratory for discussion. This research was supported by Grant-in-aid for Young Scientists (A), JSPS, Japan.

Author contributions

T. U. performed the imaging experiments, analyzed the data, and wrote the paper; T. H. designed the study, performed the behavioural analyses, and wrote the paper; R. Y. and A. S. performed the imaging analyses; G. T. performed epistasis analyses; K. Y. and Y. I. performed the behavioural experiments and analyzed the data; and T. I. designed the experiments and developed some of the analytical tools.

Additional information

Supplementary Information accompanies this paper at <http://www.nature.com/scientificreports>

Competing financial interests: The authors declare no competing financial interests.

License: This work is licensed under a Creative Commons Attribution-NonCommercial-ShareAlike 3.0 Unported License. To view a copy of this license, visit <http://creativecommons.org/licenses/by-nc-sa/3.0/>

How to cite this article: Uozumi, T. *et al.* Temporally-regulated quick activation and inactivation of Ras is important for olfactory behaviour. *Sci. Rep.* **2**, 500; DOI:10.1038/srep00500 (2012).